Article

Conventional Hydrothermal Synthesis of MFI Zeolite in Methanol Solution

Jin Quan Tao, Yi Jing Jia, Yan Cui, Tian Yu Bai, Xi Nan Xue, Rong Peng Yao, Ya Song Zhou, and Qiang Wei*
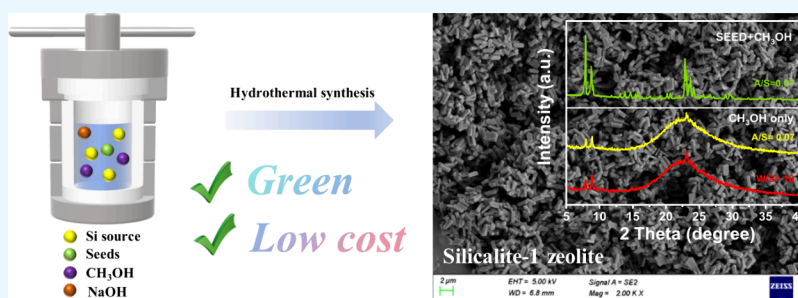
Read Online

ACCESS | Metrics & More | Article Recommendations | Supporting Information

ABSTRACT: The synthesis of zeolites through more efficient, environmentally friendly, and cost-effective methods was deemed significant in both industrial applications and academic fields. Conventional hydrothermal synthesis strategies have encountered difficulties in producing pure silica MFI zeolite (silicalite-1) under amine-free conditions. This was primarily attributed to the competitive growth of quartz, keatite, or magadiite during the crystallization process. In this work, it was found that the lack of nucleation ability was an important reason for the poor crystallization stability of the methanol solution. Well-crystallized silicalite-1 zeolites with uniform particle sizes were achieved through the cooperative guidance of methanol and seed crystals. Large-scale experiments with silicalite-1 zeolite demonstrated good reproducibility. Combined with the TG-IR and N_2 adsorption−desorption results, it was observed that, when an extremely small amount of seed (0.97 wt %) was introduced, methanol could play a role as a crystallization promoter in the hydrothermal synthesis system. Furthermore, a lower alkaline-to-silica ratio and water-to-silica ratio were conducive to the progression of the crystallization process. In summary, this work presented a hydrothermal synthesis strategy for the synthesis of silicalite-1 zeolite in a methanol solution without the need for a large amount of seeds and provided an effective pathway for the low-cost, large-scale production of silicalite-1 zeolite.

1. INTRODUCTION

MFI zeolite, characterized by a well-developed and uniform pore structure, large surface area, tunable acidity, and excellent thermal and hydrothermal stability, is an important catalytic material widely applied in fields such as petrochemical and coal chemical industries.[1−5] As an important category of zeolites, pure silica zeolites (silicalite-1) find extensive applications in various fields such as adsorbents and catalyst supports.[6−8] Generally, the conventional synthesis of silicalite-1 zeolite often relies on substantial amounts of organic amine template agents, which result in high production costs and environmental pollution.[9] Therefore, in recent years, there has been extensive research on environmentally friendly synthesis routes for the silicalite-1 zeolite. Flanigen et al.[10] synthesized silicalite-1 zeolite without aluminum. Zhang et al. initially reported instances of synthesizing MFI zeolite without OSDAs, achieved by fine-tuning crystallization conditions.[11] The addition of solid or liquid seeds in amine-free conditions can accelerate crystallization and improve the product's crystallinity.[12] The difficulty of zeolite crystallization increases with

the SiO_2/Al_2O_3 ratio. In previously reported studies, MFI zeolite synthesized without OSDAs remained limited to medium to low SiO_2/Al_2O_3 ratios.[13] However, high-silica or silicalite-1 has been widely used in catalytic reactions due to its significant catalytic stability and selectivity for the target product.[14,15] Several efforts have been made in the direction of amine-free synthesis, such as solid-state methods, seeding approaches, and hydrothermal synthesis.[16−18] Solid-state methods often face challenges related to crystallinity and particle size, as they are influenced by grinding conditions, leading to slow industrial progress. Seeding methods can raise costs and environmental pressures when used with a large number of seeds. The optimal crystallization conditions in
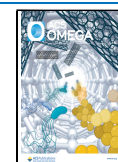
hydrothermal synthesis tend to be narrow, leading to poor system stability and often requiring a substantial amount of seed addition. These issues, which include accommodating variations in raw materials and broadening crystallization conditions, are identified as fatal challenges for industrial-scale amplification experiments.[19,20]

Zeolite crystallization is a complex self-assembly synthesis system involving multiple behaviors and colloid interactions.[21] The system mechanism of crystallization remains a subject of debate, and the crystallization process remains a mystery. Currently, it is widely believed that the growth of zeolites primarily follows both classical and nonclassical mechanisms, including particle attachment. In 2019, a study conducted by Xiao et al. successfully synthesized silicalite-1 zeolite in a solvent-free system through the synergistic action of ethanol and seeds.[18] Xiao et al. observed that ethanol exhibited relatively weak interactions with the MFI framework in the presence of solvents, primarily acting as a framework filler. Notably, ethanol could be recycled by recovering the crystallization mother liquor. Furthermore, inorganic cations such as Na^+ or K^+ from alkaline sources are often considered effective modifiers. A study by Ye et al.[22] revealed that Na^+ could promote the formation of the MFI structure but inhibit the formation of highly compact structural precursors, offering a potential method to reduce waste in the production of the MFI zeolite phase. Yue et al. successfully synthesized high-silica MFI zeolite with a silica-to-aluminum ratio of 200 using a hydrothermal method with ethanol as a template while the seed addition was 10 wt %.[23] Thermogravimetric analysis (TG) results indicated that ethanol played a role as a framework filler in the hydrothermal system and that it could be removed and repeatedly reused through washing. This work undeniably represents a significant breakthrough in the hydrothermal synthesis of high-silica zeolite in an ethanol system. However, whether the introduction of a large number of seeds can replace alcohol as the dominant factor in crystallization remains unreported. The role of alcohols in the synergistic action of alcohol and seeds has been a challenging issue. Unfortunately, to date, there has been no systematic study addressing this matter.

In recent years, our research group has successfully reported cases of synergistic synthesis of high-silica ($SiO_2/Al_2O_3 = 300$) MFI zeolite under hydrothermal conditions using ethanol and minute seed crystals.[24,25] The experimental results have been scaled up to 1 L (1L) and 2 L (2L) levels, demonstrating excellent reproducibility. Building on this foundation, we embarked on the synthesis of zeolite silicalite-1 in a low-carbon alcohol system. Herein, we reported a successful example of synthesizing silicalite-1 zeolite in a hydrothermal system by introducing a trace amount of seeds in a methanol solution. In this work, a detailed investigation was conducted of the crystallization-promoting effect of alcohols. The silica-to-aluminum ratio of MFI zeolite synthesized in the methanol solution was successfully widened to pure silica.

2. EXPERIMENTAL SECTION

2.1. Materials.
The chemicals used in this work include 30% alkaline silica sol (SiO_2, 30 wt %, aqueous solution), methanol (CH_3OH, 99.5%, analytical grade, Aladdin), TPAOH (25 wt % in aqueous solution, AR grade, Aladdin), TEOS (AR grade, Sinopharm), NaOH (AR grade, Aladdin), and deionized water (H_2O).

2.2. Preparation of Seeding Suspension.
A typical silicalite-1 seed was obtained as follows. First, TPAOH and H_2O were mixed and stirred for 1 h. Then, TEOS was added, and the vigorous stirring continued for 4 h to obtain a crystallization gel. The molar ratio of the mixture was 70 SiO_2:25 TPAOH:3000 H_2O. The mixture was placed in a stainless steel reactor and heated under rotation at 95 °C for 48 h. The product was cooled, dried, and calcined at 550 °C for 4 h. Afterward, 270 g of deionized water was added to obtain a suspension of silicalite-1 zeolite seeds. The obtained silicalite-1 suspension was directly used as seeds (Figure.S1).

2.3. Preparation of Silicalite-1 Samples.
NaOH was dissolved in deionized water, after 10 min of stirring, a specific quantity of 10% NaOH solution was slowly added to a 120 g alkaline silica sol, while vigorous stirring was maintained for 1 h. Then, a small amount of seed crystals (0.5−5.0 wt %, $mSiO_2$ in the seed crystals/$mSiO_2$ in the feed) was added; the stirring was continued for 1 h and labeled as gel A. Under vigorous stirring, methanol was simultaneously added dropwise into gel A. After the complete addition, the stirring was continued for 2 h to obtain the mixed gel. The molar ratio in the mixed gel was as follows: $1SiO_2$:(1.08−5.45) CH_3OH:(0.03−0.12) Na_2O:(5−35) H_2O. The mixed gel was placed in a 250 mL polytetrafluoroethylene-lined stainless steel reaction vessel and crystallized at 170 °C for 10−50 h. After cooling, filtration, drying and calcination at 550 °C for 4 h in an air atmosphere (heating rate of 2 °C per minute), silicalite-1 zeolite samples were obtained, labeled as M-S-1. For comparison, the silicalite-1 sample synthesized solely with the addition of seed was labeled as SEED-S-1. First, TPAOH and H_2O were mixed and stirred for 1 h. Then, TEOS was added, and the vigorous stirring continued for 4 h to obtain a crystallization gel. The molar ratio of the mixture was 70 SiO_2:25 TPAOH:3000 H_2O. The mixture was placed in a stainless steel reactor and heated under rotation at 95 °C for 48 h. The SEED-S-1 product was cooled, dried, and calcined at 550 °C for 4 h. Silicalite-1 was synthesized using TPAOH and TEOS following the method in section 2.2, labeled as TPA-S-1.

2.4. Catalyst Characterization.
The characterization techniques involved in this work included X-ray diffraction (XRD), N_2 adsorption−desorption, thermogravimetric analysis (TG), thermogravimetric analysis/infrared spectroscopy coupling (TG-IR), scanning eletron microscopy (SEM), high-resolution transmission electron microscopy (HRTEM), UV Raman, ammonia temperature-programmed desorption (NH_3-TPD), pyridine adsorption followed by infrared spectroscopy (Py-IR), inductively coupled plasma optical emission spectrometer (ICP-OES), and X-ray photoelectron spectroscopy (XPS). Details of various techniques and the scaled-up experiment are listed in the Supporting Information.

2.5. Computational Models and Methods.
To investigate the difficulty of defect site formation in different systems, theoretical calculations were conducted with Materials Studio software. The MFI structure model without defect was retrieved from the IZA structure database; the defective MFI structure is obtained by removing the Si atom from the T1 position and adding hydrogen to the bridging oxygen that was originally connected to it. The methanol molecule was added to the zeolite channels using the GCMC method, employing the Sorption module, while the relatively large TPA^+ was manually added at the channel intersections. The calculations using the GCMC method were performed using the Metropolis method and employed the cvff force field.[31] DFT

calculations were performed using the DMol[3] module to determine precise adsorption configurations and energies. These calculations utilized the Perdew−Burke−Ernzerhof (PBE) functional under the Generalized Gradient Approximation (GGA), double numeric orbital basis sets with polarization functions (DNP) of version 4.4, and the inclusion of Grimme dispersion correction.[32] The orbital cutoff value set in all of the DFT calculations was 4 Å, and the k-points were set to $1 \times 1 \times 1$. Throughout the geometry optimization process, none of the atomic positions were constrained.

Based on the computational results, all guest molecules (methanol and TPA[+]) interacted with the MFI framework. Consequently, the total interaction energy (ΔE_{int}) between all guest molecules and the MFI framework was calculated. ΔE_{int} was determined by subtracting the total energy of the system after adsorption ($E_{MFI\text{-}adsorbates}$) from the energy of the MFI crystal cell (E_{MFI}) and the total energy of all guest molecules ($E_{adsorbates}$), that is, $\Delta E_{int} = E_{MFI\text{-}adsorbates} - E_{MFI} - E_{adsorbates}$.[18,25]

3. RESULT AND DISCUSSION

3.1. Synthesis of MFI Zeolite in Single Methanol Solution.
The synthesis of silicalite-1 zeolite imposes more stringent requirements (the directing ability of the template, system alkalinity, and water-to-silica ratio were taken into consideration) on crystallization conditions, crystal growth rate, structural stability, and solvent selectivity. With the increase in the silica-to-alumina ratio of MFI zeolites, the relative content of silicon atoms increases, leading to a slowing down of the crystal growth rate and phase transformation during crystallization. Among numerous influencing factors, we first explored the crystallization conditions for synthesizing MFI zeolites in a single methanol solution by varying parameters such as the methanol-to-silica ratio (M/S ratio), alkali-to-silica ratio (A/S ratio), and water-to-silica ratio (W/S ratio). The experimental results indicated that, with the increase in the feedstock silica-to-alumina ratio, the relative crystallinity (R.C.%) of MFI zeolites showed a decreasing trend. The optimal A/S ratio for MFI zeolites exhibited a decreasing trend, while the range of W/S ratio narrowed, and the optimal W/S ratio decreased with the increase in the silica-to-alumina ratio (Figures S2−S4). The experiments described above indicate that MFI zeolites with a silica-to-aluminum ratio of 30−120 could be synthesized in a single methanol solution, suggesting that methanol may have played a directing role similar to TPAOH during the crystallization process. Based on this trend, we attempted to synthesize silicalite-1 zeolite in a methanol solution. The experimental results showed that when the W/S ratio decreased from 30 to 16, the R.C.% of silicalite-1 zeolite increased to 20%; when the A/S ratio decreased from 0.1 to 0.07, the R.C.% of silicalite-1 zeolite increased to 6.7% (Figures S5−S7). The above experiments indicate that high-crystallinity silicalite-1 zeolite cannot be directly synthesized in a single methanol solution. To address this issue, we introduced silicalite-1 seeds, resulting in a significant increase in the crystallinity of silicalite-1 zeolite (Figure 1).

3.2. Thermal Properties and Surface Texture.
In order to investigate the local environment of alcohol molecules and the thermal stability of silicalite-1 zeolite, thermal analysis was performed on the synthesized zeolite at a heating rate of 10 °C/min up to 700 °C. The TG curves are shown in Figure 2a. The primary mass loss of M-S-1 occurred between 350 and 475 °C. Between 50 and 200 °C, the main processes involved
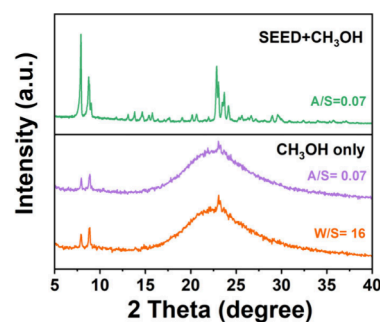

Figure 1. XRD pattern of silicalite-1 zeolite synthesized with seed addition in the methanol system.
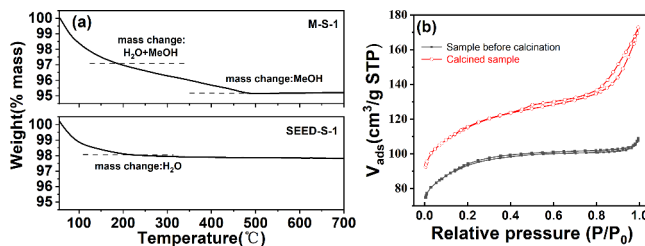

Figure 2. (a) TG curve of M-S-1 zeolite. (b) Adsorption and desorption isotherms of M-S-1 zeolite.

dehydration and partial methanol removal, while between 200 and 475 °C, methanol removal and carbon decomposition occurred. To investigate the substances causing mass loss during the TG process, TG-IR analysis of the residues was conducted, as shown in Figure 3. During the heating process up to 700 °C, the desorption processes of water (1510 cm^{-1}) and methanol (2980 cm^{-1}) were continuously observed. As the temperature increased from room temperature to 200 °C, only water molecules were detected in the IR spectra of the gas-phase products. At 200 °C, the peak at 1510 cm^{-1} completely disappeared, indicating that the water molecules in the channels of the MFI zeolite framework had been completely removed. During the temperature increase to 475 °C, a strong peak appeared only at 2980 cm^{-1}, indicating the removal of methanol molecules at this stage. As the temperature continued to rise to 700 °C, no significant peaks were observed, suggesting that the water and methanol molecules within the MFI framework had been completely removed. This corresponds to the two stages of mass loss (50−200 °C and 200−475 °C) observed in the TG results. The TG-IR results indicated that the mass loss of the M-S-1 zeolite during heating was related to water and methanol. The N$_2$ adsorption−desorption isotherms of M-S-1 zeolite before and after calcination exhibited typical type IV adsorption isotherms (Figure 2b), indicating that the synthesized silicalite-1 zeolite had a mesoporous structure. The specific surface area before calcination was 272 m^2/g. The micropore surface area was 223 m^2/g, and the average pore diameter was 2.87 nm. After calcination, the total surface area increased to 342 m^2/g, the micropore surface area was 289 m^2/g, and the average pore diameter was 2.49 nm (Table S1), indicating an increase in the microporous structure of the silicalite-1 zeolite after calcination. According to Groen,[26] MFI zeolites undergo a fluid-to-crystal phase transition during N$_2$ adsorption, resulting in additional pore volume at around 2 nm. Comparing the pore structure changes before and after calcination of sample M-S-1, it was found that the specific surface area of the M-S-1 sample
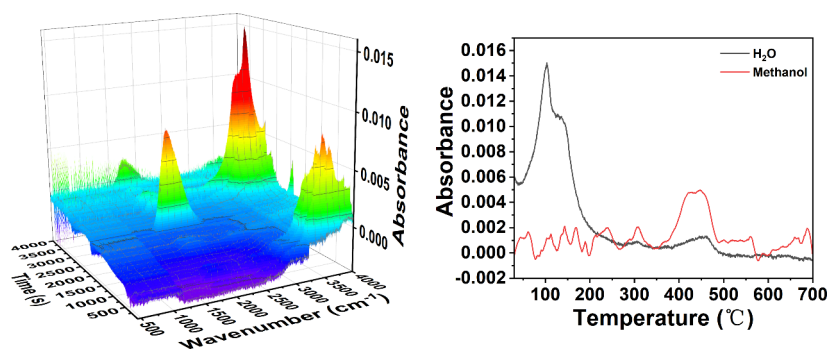
Figure 3. TG-IR pattern of the M-S-1 zeolite.

increased significantly after calcination. The reduction in pore size was indicative of more micropore structures being exposed after calcination; since no organic amine template agent was used in the synthesis system, it was evident that methanol molecules were removed from the micropore channels of the zeolite through calcination. This is consistent with the TG curve, which showed that complete methanol removal only occurred at high temperatures. The N_2 adsorption−desorption test also indicated that the degassing process at temperatures below 220 °C was unable to completely eliminate methanol. It was found that methanol molecules resided within the zeolite channels and required heating to relatively high temperature to desorb; methanol played a crystallization promoter role, which was related to the strong interaction forces between methanol and the zeolite framework.

3.3. The Exploration of Optimal Crystallization Conditions. Obtaining high crystallinity pure-phase silicalite-1 zeolite is challenging under conditions of a high water-to-silica ratio (W/S), as the presence of a large amount of water molecules weakens the interaction between the template agent and the MFI framework. As shown in Figure S8, when the W/S ratio decreased from 31 to 26, weak characteristic peaks of silicalite-1 zeolite appeared in the XRD pattern. The SEM images of silicalite-1 zeolite synthesized at different crystallization times under the W/S ratio of 26 are shown in Figure 4A. Further reducing the W/S ratio to 16 resulted in a decrease
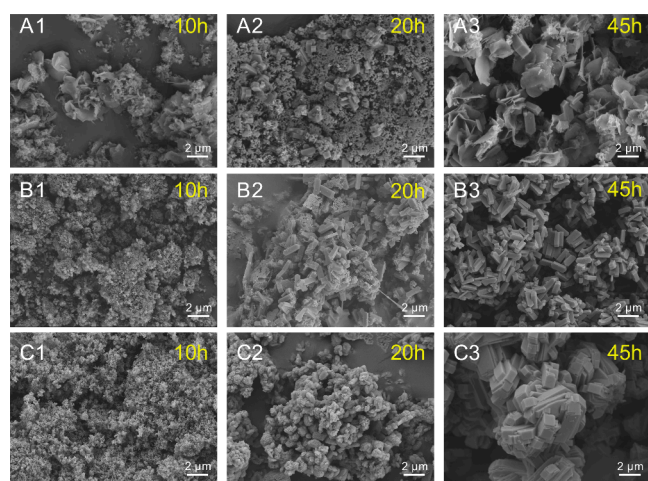

Figure 4. SEM images of the M-S-1 zeolites synthesized at 170 °C for different times: (A) 0.97 wt % seed addition amount and W/S = 26, (B) 0.97 wt % seed addition amount and W/S = 8, (C) 5 wt % seed addition amount and W/S = 8.

in the intensity of the characteristic peaks of magadiite, while the intensity of the silicalite-1 zeolite characteristic peaks increased. However, due to the sensitivity of alkaline silica sol stability to factors such as temperature and concentration, aggregation and precipitation were prone to occur when in contact with high concentrations of alcohols, leading to experimental failure. When the W/S ratio decreased to 12, the alkaline silica sol−gel system lost its colloidal suspension properties, resulting in irreversible precipitation (Figures S9, S10). Controlling the stirring temperature effectively avoided the precipitation phenomenon of the alkaline silica sol−gel system when the W/S ratio was lowered. A pure-phase silicalite-1 zeolite sample was obtained when the stirring temperature was 20 °C and the W/S ratio was 8 (Figure S11); the SEM images are shown in Figure 4B. The addition of crystal seeds had a significant effect on the methanol crystallization system. When the crystal seed addition was 0.97 wt %, silicalite-1 zeolite exhibited a well-dispersed regular hexagonal prism morphology, with a particle size of approximately 2 μm. Increasing the crystal seed addition to 5 wt % resulted in silicalite-1 zeolite products with twinned crystal morphology and significantly increased particle size (Figure 4C). The XRD pattern showed that the intensity of characteristic peaks of M-S-1 (5 wt %) was significantly higher than that of M-S-1 (0.97%) samples (Figure S12), which was interpreted as an acceleration of crystallization under the same crystallization time with an increase in the amount of crystal seeds. Under conditions devoid of TPA$^+$, the crystallization was directed toward the less demanding magadiite crystallographic orientation, consistent with the findings reported by Ren et al.[27] In the methanol-seed crystallization system, the minute quantity of seed added played a role identical with that of the nucleus during the early stages of crystallization. However, it was insufficient to guide the oriented growth of the crystals. The addition of methanol had the effect of inhibiting the growth of magadiite crystallographic impurity phases and exerting the function of either SDAs or fillers, thereby promoting the rapid growth of crystals. It is worth noting that the synthesis of silicalite-1 zeolite in the methanol solution needed to be conducted under conditions of low stirring temperature and a low W/S ratio.

Figures 5 and 6 display SEM and TEM images of silicalite-1 zeolites synthesized under different methanol-to-silica ratios (M/S ratio). When the M/S ratio was 1.82, a significant amount of layered magadiite impurity phases was present in the product, with a small quantity of silicalite-1 crystals adhering to the surface of the layered magadiite. The silicalite-1 particle size was approximately 1 μm. When the M/S ratio was increased to 2.53, the presence of the layered magadiite
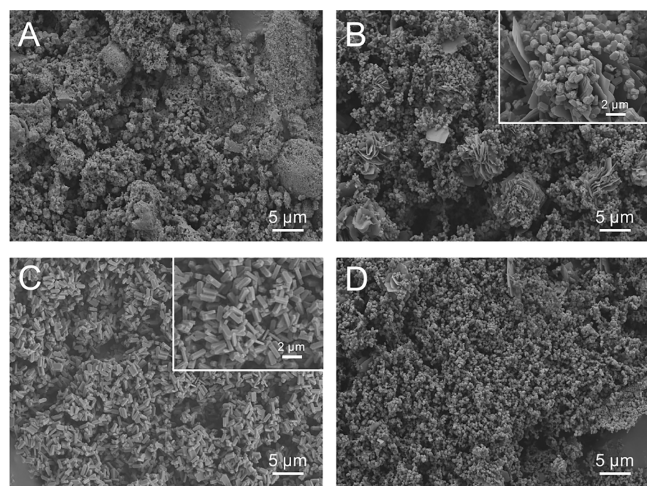
Figure 5. SEM images of samples synthesized under different methanol-silica ratio conditions $n(\text{methanol})/n(\text{SiO}_2) = x$, $x = 1.82$ (A), $x = 2.53$ (B), $x = 3.88$ (C), $x = 5.45$ (D).
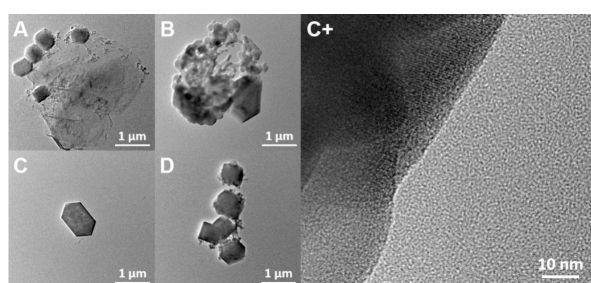

Figure 6. TEM images of samples under different methanol−silica ratio conditions $n(\text{methanol})/n(\text{SiO}_2) = x$, $x = 1.82$ (A), $x = 2.53$ (B), $x = 3.88$ (C), $x = 5.45$ (D).

phase noticeably decreased, and there were no apparent impurity peaks in the XRD pattern (Figure 7a), indicating the
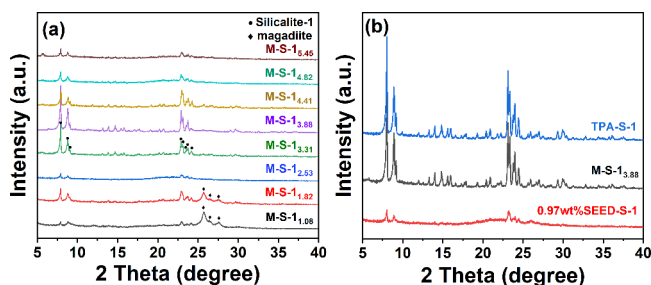

Figure 7. XRD pattern of samples synthesized under different methanol−silica ratio conditions (a) and samples synthesized under different template agents (b).

presence of amorphous substances at this point. When the M/S ratio was further increased to 3.88, the product achieved the highest relative crystallinity. The crystals exhibited a regular ac-plane-oriented hexagonal prism morphology and were in a monodisperse state. However, when the M/S ratio continued to rise to 5.45, a significant amount of amorphous substances reappeared in the product. This suggests that an excessive amount of methanol can inhibit the crystallization reaction of silicalite-1 zeolite. The reason may be that an excess of methanol affects the solubility of silicate species in water, thereby inhibiting crystal growth. In Figure 7b, except for 0.97

wt % SEED-S-1, all other samples displayed characteristic peaks at $2\theta = 7-9°$ and $22-25°$, indicating the formation of a crystalline MFI structure with orthorhombic symmetry. This indicates that adding only 0.97 wt % seed crystals is insufficient to synthesize well-crystalline silicalite-1 products.

The alkali-to-silica ratio (A/S ratio) is an important parameter during the hydrothermal synthesis process. When the amount of sodium hydroxide is increased, samples obtained at different hydrothermal reaction times (10−50 h) were compared using eq S1, by analyzing the peak intensities of the five sharpest peaks in the MFI structure at $2\theta = 7-9°$ and $22-25°$ with respect to the intensity of the TPA-S-1 sample. This calculation was used to determine the R.C.% of the zeolite (Table S2). Figure 8a displayed the XRD pattern of
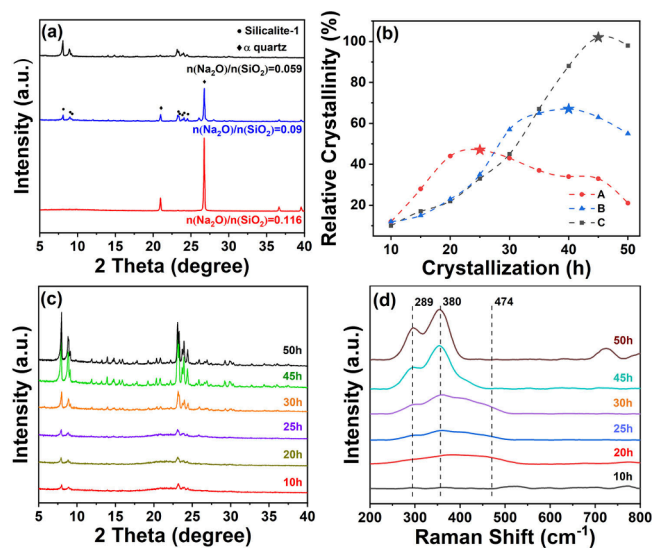

Figure 8. (a) XRD pattern of silicalite-1 zeolites. (b) Crystallization curve under different alkali-to-silica ratio conditions, $n(\text{Na}_2\text{O})/n(\text{SiO}_2) = x$, $x = 0.116$ (A), 0.09 (B), 0.059 (C). (c) XRD pattern of samples synthesized with different crystallization times and (d) UV Raman spectra.

silicalite-1 zeolites synthesized at a hydrothermal reaction time of 45 h under different A/S ratios. The XRD results indicated that the growth of α-quartz was significantly inhibited as the A/S ratio was decreased. When the A/S ratio was 0.059, a high crystallinity silicalite-1 zeolite product with a pure phase was obtained. Table S2 revealed that, as the hydrothermal reaction time increased from 10 to 50 h, the crystallinity of the product significantly increased. The optimal crystallization time (25 h, 40 h, 45 h) was extended with an increase in the A/S ratio. As the A/S ratio was decreased, the relative crystallinity of the product increased, and the growth of α-quartz was inhibited. When the A/S ratio was 0.116, the R.C.% reached its maximum at 47% after 25 h. When the A/S ratio was reduced to 0.09, the crystallinity reached its maximum of 67% after 40 h. Further lowering the A/S ratio to 0.059 resulted in a product with a crystallinity of 102% after 45 h (Figure 8b). Therefore, reducing the A/S ratio was found to be favorable for the crystallization of silicalite-1 zeolites in the alcohol-crystal seed system. In conclusion, lowering the A/S ratio reduced the crystallization rate of the system but enhanced the crystallization stability of the system. The XRD patterns of samples crystallized at different times with a A/S ratio of 0.059 are shown in Figure 8c, indicating that the intensity of character-

istic peaks increased with the increase in crystallization time within 50 h. The crystallization process was tracked by using UV Raman spectroscopy, as depicted in Figure 8d. Prior to crystallization, the sample exhibited two distinct bands at approximately 380 cm^{-1} (representing 5MRs) and 474 cm^{-1} (representing 4MRs). After 25 h of crystallization, a band associated with 6MRs appeared at 289 cm^{-1}. When the crystallization time reached 45 h, the band at 474 cm^{-1} completely disappeared. This may imply a change in the crystallization of active building units during the crystallization process. After 45 h of crystallization, well-crystallized silicalite-1 zeolites were successfully obtained.

3.4. Scaling-up Experiment and Acidic Properties of Silicalite-1.
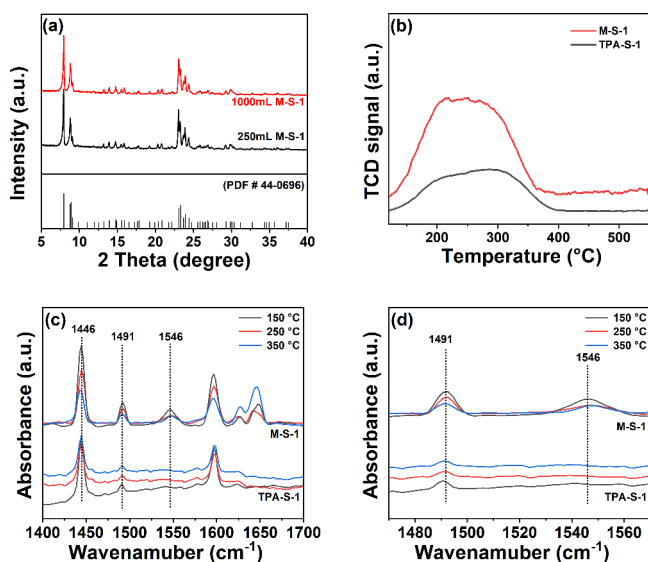The XRD pattern (Figure 9a) revealed that the

Figure 9. (a) XRD pattern, (b) NH$_3$-TPD spectra, (c) Py-IR spectra, and (d) Py-IR magnified spectra of M-S-1 and TPA-S-1.

scaled-up silicalite-1 zeolite exhibited typical MFI structure diffraction peaks. The acidity of the MFI zeolite was determined by Py-IR and NH$_3$-TPD. NH$_3$-TPD results (Figure 9b) showed that the NH$_3$ desorption curve of TPA-S-1 zeolite was nearly a straight line, indicating very weak acidity in the silicalite-1 zeolite. The NH$_3$ desorption peak of M-S-1 zeolite exhibited a slight increase, possibly due to the higher number of framework defect sites in silicalite-1 synthesized in the methanol solution. Further investigation is required. The total acidity of silicalite-1 zeolite significantly increased, and the peaks below 300 °C were attributed to ammonia desorption from weak acid sites, while peaks above 300 °C were assigned to ammonia desorption from stronger acid sites. The total acidity of the silicalite-1 zeolite was 0.0071 and 0.0132 mmol/g, respectively. Py-IR results (Figure 9c, Figure 9d, and Table S3) showed a characteristic peak at 1450 cm^{-1}, indicating Lewis acid sites, which was present in all two types of molecular sieve samples. However, M-S-1 samples exhibited a more pronounced absorption peak at 1450 cm^{-1}, suggesting the presence of stronger Lewis acid centers. Additionally, the peak at 1540 cm^{-1} was attributed to Bronsted acid sites, and the peak at 1490 cm^{-1} was attributed to both Lewis and Bronsted acid sites. M-S-1 exhibited a stronger absorption peak at 1540 cm^{-1}, indicating the presence of stronger Bronsted acid centers capable of chemical adsorption of C$_5$H$_5$N. The

experimental results indicate that the M-S-1 zeolite samples synthesized using methanol possess a higher abundance of acid sites. According to Table S4, it was observed that the silicalite-1 samples had an extremely low content of Al impurities; this phenomenon is speculated to be related to the generation of more framework defect sites[28−30] during the synthesis process in volving methanol.

Theoretical simulations explain the difference in silicon hydroxyl content between the methanol and TPA systems (Figure 10). In the methanol solution, methanol molecules can
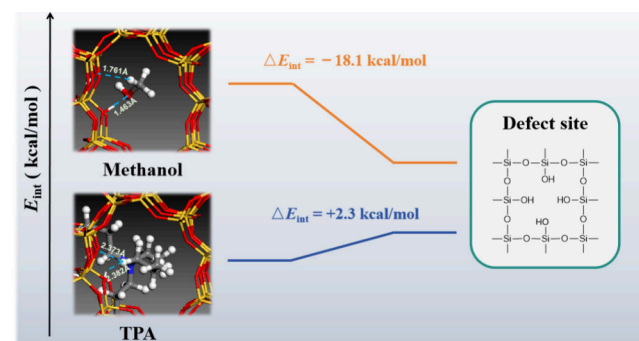

Figure 10. Schematic representation of a guest molecule at the structural defects within MFI unit cells.

form hydrogen bonds with hydroxyl groups at defect sites. Compared to systems without defect sites, the interaction energy between methanol molecules and the framework changes by −18.1 kcal/mol, indicating the stabilizing effect of methanol on framework defect sites. Conversely, the presence of defect sites is not conducive to the energy localization of TPA. Within defect sites, the distances between oxygen and hydrogen atoms closest to the H atom on TPA are 2.373 and 2.382 Å, respectively, resulting in repulsion between TPA and hydroxyl groups attributed to TPA's hydrophobicity. Therefore, silicalite-1 synthesized in the methanol solution exhibits a higher content of silicon hydroxyl groups. Moreover, Figure 11 depicts the catalytic performance of Fe/M-S-1 and Fe/TPA-S-1 zeolite samples modified by impregnation in the chichibabin condensation reaction. The chichibabin condensation reaction is a typical acid-catalyzed reaction, it was carried out in a continuous high-temperature hydrothermal environment. This resulted in more stringent requirements for the thermal stability and hydrothermal stability of the catalyst in the chichibabin condensation reaction. The acidic properties of Fe/M-S-1 and Fe/TPA-S-1 samples are shown in Table S3. Fe/M-S-1 exhibited a greater abundance of acidic sites. This phenomenon could be explained by the presence of more defect sites in the M-S-1 sample, which facilitated the bonding of Fe with the zeolite framework, thereby forming acidic sites. The reaction evaluation results indicated that Fe/TPA-S-1 and Fe/M-S-1 exhibited comparable initial conversion rates at the same reaction temperature. The total carbon conversion rates within 3 h of reaction were 62.1% and 61.5%, respectively. Considering the higher space−time conversion rate and lower synthesis cost, M-S-1 samples showed significant potential in practical production applications compared to TPA-S-1 samples.
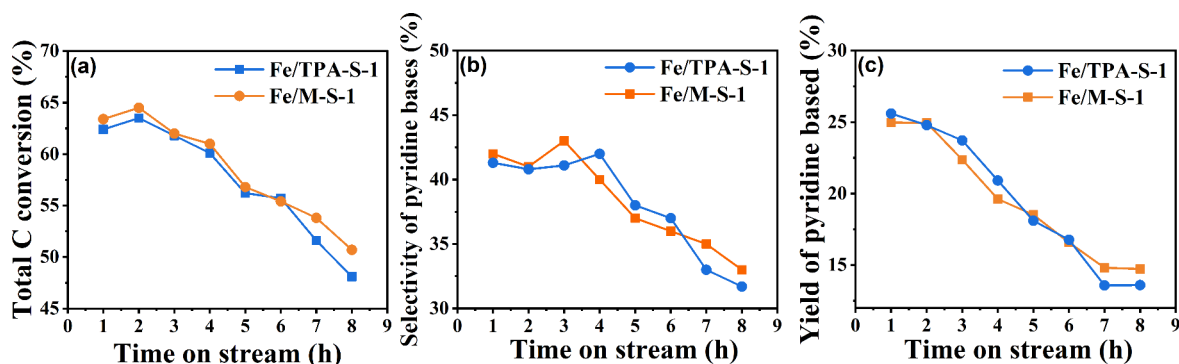
Figure 11. Total carbon conversion rate (a), pyridine base selectivity (b), and pyridine base yield (c) of Fe/TPA-S-1 and Fe/M-S-1 catalysts in the chichibabin condensation reaction.

4. CONCLUSION

The role of methanol is often overlooked in hydrothermal synthesis due to the addition of a large quantity of seed crystals. In this work, we have demonstrated that methanol can serve as an effective crystallization promoter in a hydrothermal synthesis system; due to the lack of a tetrahedral structure similar to TPA^+ in methanol, its poor nucleation ability in the early stages of crystallization prevents effective self-assembly processes, leading to poor crystallinity of zeolite products. The introduction of trace amounts of crystal seeds can significantly enhance the crystallinity of silicalite-1 zeolites synthesized in methanol solution. Characterizations indicate that, with extremely low seed crystal input, methanol can effectively promote the crystallization of MFI siliceous zeolite and inhibit the growth of impurity phases. Lower water-to-silica ratios favor crystallization. The scale-up experiment indicated that the silicalite-1 product exhibits good crystallinity and reproducibility. The method of using methanol in combination with trace amounts of crystal seeds has expanded the silica-to-aluminum ratio range for hydrothermal synthesis of MFI zeolites to pure silica in methanol solution. The experimental results demonstrate significant research value and broad prospects for industrial application.

ASSOCIATED CONTENT

Supporting Information

The Supporting Information is available free of charge at https://pubs.acs.org/doi/10.1021/acsomega.4c04513.

> Catalyst characterization details, reaction evaluation conditions, additional XRD characterization, SEM images, ICP, XPS, Py-IR, summary of relative crystallinity, pore structure, element content, and acid properties of M-S-1 zeolites (PDF)

AUTHOR INFORMATION

Corresponding Author

Qiang Wei — *State Key Laboratory of Heavy Oil Processing, China University of Petroleum-Beijing, Beijing 102249, China;* ◉ orcid.org/0000-0002-4631-0640; Phone: +86-13601228168; Email: qwei@cup.edu.cn; Fax: +86-13601228168

Authors

Jin Quan Tao — *State Key Laboratory of Heavy Oil Processing, China University of Petroleum-Beijing, Beijing*
102249, China; PetroChina Petrochemical Research Institute, Beijing 102206, China; ◉ orcid.org/0009-0002-7383-2185

Yi Jing Jia — *State Key Laboratory of Heavy Oil Processing, China University of Petroleum-Beijing, Beijing 102249, China*

Yan Cui — *PetroChina Petrochemical Research Institute, Beijing 102206, China*

Tian Yu Bai — *State Key Laboratory of Heavy Oil Processing, China University of Petroleum-Beijing, Beijing 102249, China*

Xi Nan Xue — *State Key Laboratory of Heavy Oil Processing, China University of Petroleum-Beijing, Beijing 102249, China*

Rong Peng Yao — *State Key Laboratory of Heavy Oil Processing, China University of Petroleum-Beijing, Beijing 102249, China*

Ya Song Zhou — *State Key Laboratory of Heavy Oil Processing, China University of Petroleum-Beijing, Beijing 102249, China;* ◉ orcid.org/0000-0003-4276-9814

Complete contact information is available at:
https://pubs.acs.org/10.1021/acsomega.4c04513

Notes

The authors declare no competing financial interest.

REFERENCES

(1) Xie, D. New Insight from an Old Concept for Zeolites. *Science* **2021**, *373* (6550), 28−28.

(2) Pham, T. N.; Nguyen, V.; Nguyen-Phu, H.; Wang, B.; Crossley, S. Influence of Brønsted Acid Site Proximity on Alkane Cracking in MFI Zeolites. *ACS Catal.* **2023**, *13* (2), 1359−1370.

(3) Davis, M. E. Ordered Porous Materials for Emerging Applications. *Nature* **2002**, *417* (6891), 813.

(4) Zhang, X.; Liu, D.; Xu, D.; Asahina, S.; Cychosz, K. A.; Agrawal, K. V.; Al Wahedi, Y.; Bhan, A.; Al Hashimi, S.; Terasaki, O.; Thommes, M.; Tsapatsis, M. Synthesis of Self-Pillared Zeolite Nanosheets by Repetitive Branching. *Science* **2012**, *336* (6089), 1684−1687.

(5) Cundy, C. S.; Cox, P. A. The Hydrothermal Synthesis of Zeolites: History and Development from the Earliest Days to the Present Time. *Chem. Rev.* **2003**, *103* (3), 663−702.

(6) Wu, Q.; Meng, X.; Gao, X.; Xiao, F.-S. Solvent-Free Synthesis of Zeolites: Mechanism and Utility. *Acc. Chem. Res.* **2018**, *51* (6), 1396−1403.

(7) Bereciartua, P. J.; Cantín, Á.; Corma, A.; Jordá, J. L.; Palomino, M.; Rey, F.; Valencia, S.; Corcoran, E. W.; Kortunov, P.; Ravikovitch, P. I.; Burton, A.; Yoon, C.; Wang, Y.; Paur, C.; Guzman, J.; Bishop, A. R.; Casty, G. L. Control of Zeolite Framework Flexibility and Pore Topology for Separation of Ethane and Ethylene. *Science* **2017**, *358* (6366), 1068−1071.

(8) Nimlos, C. T.; Hoffman, A. J.; Hur, Y. G.; Lee, B. J.; Di Iorio, J. R.; Hibbitts, D. D.; Gounder, R. Experimental and Theoretical Assessments of Aluminum Proximity in MFI Zeolites and Its Alteration by Organic and Inorganic Structure-Directing Agents. *Chem. Mater.* **2020**, *32* (21), 9277−9298.

(9) Iyoki, K.; Itabashi, K.; Okubo, T. Progress in Seed-Assisted Synthesis of Zeolites without Using Organic Structure-Directing Agents. *Microporous Mesoporous Mater.* **2014**, *189*, 22−30.

(10) Flanigen, E. M.; Bennett, J. M.; Grose, R. W.; Cohen, J. P.; Patton, R. L.; Kirchner, R. M.; Smith, J. V. Silicalite, a New Hydrophobic Crystalline Silica Molecular Sieve. *Nature* **1978**, *271* (5645), 512−516.

(11) Zhang, B.; Douthwaite, M.; Liu, Q.; Zhang, C.; Wu, Q.; Shi, R.; Wu, P.; Liu, K.; Wang, Z.; Lin, W.; Cheng, H.; Ma, D.; Zhao, F.; Hutchings, G. J. Seed- and Solvent-Free Synthesis of ZSM-5 with Tuneable Si/Al Ratios for Biomass Hydrogenation. *Green Chem.* **2020**, *22* (5), 1630−1638.

(12) Cheng, C.-H.; Shantz, D. F. silicalite-1 Growth from Clear Solution: Effect of Alcohol Identity and Content on Growth Kinetics. *J. Phys. Chem. B* **2005**, *109* (41), 19116−19125.

(13) Choudhary, M. K.; Kumar, M.; Rimer, J. D. Regulating Nonclassical Pathways of silicalite-1 Crystallization through Controlled Evolution of Amorphous Precursors. *Angew. Chem., Int. Ed.* **2019**, *58* (44), 15712−15716.

(14) Niu, R.; Liu, P.; Li, W.; Wang, S.; Li, J. High Performance for Oxidation of Low-Concentration Methane Using Ultra-Low Pd in silicalite-1 Zeolite. *Microporous Mesoporous Mater.* **2019**, *284*, 235−240.

(15) Bozhilov, K. N.; Le, T. T.; Qin, Z.; Terlier, T.; Palčić, A.; Rimer, J. D.; Valtchev, V. Time-Resolved Dissolution Elucidates the Mechanism of Zeolite MFI Crystallization. *Sci. Adv.* **2021**, *7* (25), No. eabg0454.

(16) Narita, E.; Sato, K.; Okabe, T. A Convenient Method for Crystallization of Zeolite ZSM-5 by Using Seed Crystals in Acetone/Water Mixture System. *Chem. Lett.* **1984**, *13* (7), 1055−1058.

(17) Ren, N.; Bronić, J.; Jelić, T. A.; Palčić, A.; Subotić, B. Seed-Induced, Structure Directing Agent-Free Crystallization of Sub-Micrometer Zeolite ZSM-5: A Population Balance Analysis. *Cryst. Growth Des.* **2012**, *12* (4), 1736−1745.

(18) Wu, Q.; Zhu, L.; Chu, Y.; Liu, X.; Zhang, C.; Zhang, J.; Xu, H.; Xu, J.; Deng, F.; Feng, Z.; Meng, X.; Xiao, F. Sustainable Synthesis of Pure Silica Zeolites from a Combined Strategy of Zeolite Seeding and Alcohol Filling. *Angew. Chem., Int. Ed.* **2019**, *58* (35), 12138−12142.

(19) Ye, Z.; Zhao, Y.; Zhang, H.; Shi, Z.; Li, H.; Yang, X.; Wang, L.; Kong, L.; Zhang, C.; Sheng, Z.; Zhang, Y.; Tang, Y. Mesocrystal Morphology Regulation by "Alkali Metals Ion Switch": Re-Examining Zeolite Nonclassical Crystallization in Seed-Induced Process. *J. Colloid Interface Sci.* **2022**, *608*, 1366−1376.

(20) Kalita, B.; Talukdar, A. K. An Efficient Synthesis of Nanocrystalline MFI Zeolite Using Different Silica Sources: A Green Approach. *Mater. Res. Bull.* **2009**, *44* (2), 254−258.

(21) Wang, C.; Guo, H.; Leng, S.; Yu, J.; Feng, K.; Cao, L.; Huang, J. Regulation of Hydrophilicity/Hydrophobicity of Aluminosilicate Zeolites: A Review. *Crit. Rev. Solid State Mater. Sci.* **2021**, *46* (4), 330−348.

(22) Ye, Z.; Zhao, Y.; Zhang, H.; Shi, Z.; Li, H.; Yang, X.; Wang, L.; Kong, L.; Zhang, C.; Sheng, Z.; Zhang, Y.; Tang, Y. Mesocrystal Morphology Regulation by "Alkali Metals Ion Switch": Re-Examining Zeolite Nonclassical Crystallization in Seed-Induced Process. *J. Colloid Interface Sci.* **2022**, *608*, 1366−1376.

(23) Yue, J.; Li, J.; Liu, M.; Liu, W.; Li, X.; Xie, S.; Song, C.; Guo, X.; Zhu, X. Amine-Free Synthesis of High-Silica MFI Zeolite by the Conventional Hydrothermal Route. *Microporous Mesoporous Mater.* **2023**, *359*, No. 112635.

(24) Tao, J.; Cui, Y.; Zhang, Y.; Chi, K.; Zhou, Y. Synthesis of ZSM-5 Zeolite with High Si/Al Ratio in Ethanol System. *Journal of the Chinese Ceramic Society* **2021**, *49*, 2009−2016.

(25) Bai, T.; Tao, J.; Jia, Y.; Huang, W.; Yao, R.; Xue, X.; Zhou, Y.; Wei, Q. Directly Synthesis of H-Form ZSM-5 Zeolites with *n*-Butylamine in the Presence of Seed and Ethanol. *Microporous Mesoporous Mater.* **2024**, *370*, No. 113057.

(26) Groen, J. Critical Appraisal of Mesopore Characterization by Adsorption Analysis. *Appl. Catal. Gen.* **2004**, *268* (1−2), 121−125.

(27) Ren, N.; Bronić, J.; Subotić, B.; Lv, X.-C.; Yang, Z.-J.; Tang, Y. Controllable and SDA-Free Synthesis of Sub-Micrometer Sized Zeolite ZSM-5. Part 1: Influence of Alkalinity on the Structural, Particulate and Chemical Properties of the Products. *Microporous Mesoporous Mater.* **2011**, *139* (1), 197−206.

(28) Huang, H.; Zhang, M.; Chen, C.; Li, C.; Cui, Q. Catalytic Performance of Cerium Modified silicalite-1 Molecular Sieves in the Conversion of Methanol to Propene. *J. Fuel Chem. Technol.* **2016**, *44* (12), 1485−1493.

(29) Meng, X.; Yu, Q.; Gao, Y.; Zhang, Q.; Li, C.; Cui, Q. Enhanced Propene/Ethene Selectivity for Methanol Conversion over Pure Silica Zeolite: Role of Hydrogen-Bonded Silanol Groups. *Catal. Commun.* **2015**, *61*, 67−71.

(30) Radhakrishnan, S.; Lejaegere, C.; Duerinckx, K.; Lo, W.-S.; Morais, A. F.; Dom, D.; Chandran, C. V.; Hermans, I.; Martens, J. A.; Breynaert, E. Hydrogen Bonding to Oxygen in Siloxane Bonds Drives Liquid Phase Adsorption of Primary Alcohols in High-Silica Zeolites. *Mater. Horiz.* **2023**, *10*, 3702.

(31) Tang, X.; Liu, Z.; Huang, L.; Chen, W.; Li, C.; Wang, G.; Li, G.; Yi, X.; Zheng, A. Violation or Abidance of Löwenstein's Rule in Zeolites Under Synthesis Conditions? *ACS Catalysis.* **2019**, *9* (12), 10618−10625.

(32) Tang, X.; Chen, W.; Dong, W.; Liu, Z.; Yuan, J.; Xia, H.; Yi, X.; Zheng, A. Framework Aluminum Distribution in ZSM-5 Zeolite Directed by Organic Structure-directing Agents: a Theoretical Investigation. *Catalysis Today.* **2022**, *405−406*, 101−110.